

## Global Phase Diagram of a Spin-Orbital Kondo Impurity Model and the Suppression of Fermi-Liquid Scale

Y. Wang<sup>1</sup>, E. Walter<sup>2</sup>, S.-S. B. Lee<sup>2</sup>, K. M. Stadler<sup>2</sup>, J. von Delft<sup>2</sup>, A. Weichselbaum<sup>1,2</sup> and G. Kotliar<sup>1,3</sup>

<sup>1</sup>Department of Condensed Matter Physics and Materials Science, Brookhaven National Laboratory, Upton, New York 11973, USA

<sup>2</sup>Arnold Sommerfeld Center for Theoretical Physics, Center for NanoScience, and Munich Center for Quantum Science and Technology, Ludwig-Maximilians-Universität München, 80333 Munich, Germany

<sup>3</sup>Department of Physics and Astronomy, Rutgers University, Piscataway, New Jersey 08856, USA



(Received 4 November 2019; accepted 28 February 2020; published 3 April 2020)

Many correlated metallic materials are described by Landau Fermi-liquid theory at low energies, but for Hund metals the Fermi-liquid coherence scale  $T_{\text{FL}}$  is found to be surprisingly small. In this Letter, we study the simplest impurity model relevant for Hund metals, the three-channel spin-orbital Kondo model, using the numerical renormalization group (NRG) method and compute its global phase diagram. In this framework,  $T_{\text{FL}}$  becomes arbitrarily small close to two new quantum critical points that we identify by tuning the spin or spin-orbital Kondo couplings into the ferromagnetic regimes. We find quantum phase transitions to a singular Fermi-liquid or a novel non-Fermi-liquid phase. The new non-Fermi-liquid phase shows frustrated behavior involving alternating overscreenings in spin and orbital sectors, with universal power laws in the spin ( $\omega^{-1/5}$ ), orbital ( $\omega^{1/5}$ ) and spin-orbital ( $\omega^1$ ) dynamical susceptibilities. These power laws, and the NRG eigenlevel spectra, can be fully understood using conformal field theory arguments, which also clarify the nature of the non-Fermi-liquid phase.

DOI: [10.1103/PhysRevLett.124.136406](https://doi.org/10.1103/PhysRevLett.124.136406)

**Introduction.**—A very large number of correlated metallic materials are “bad metals,” namely in a broad regimes of temperature  $T$  characterized by deviations from the Landau Fermi-liquid (FL)  $T^2$  law [1] and their values of resistivity exceeding the Mott-Ioffe-Regel limit [2]. One class of bad metals are the Hund metals, i.e., 3d and 4d multiorbital systems where correlations derive from the Hund’s coupling  $J_H$  [3–7]. They include ruthenates [8–13], iron pnictides and chalcogenides [14–20]. The Landau FL quasiparticles emerge only below a coherence scale  $T_{\text{FL}}$  which is much smaller than the natural energy scales of the problem, set by the electronic bandwidth. Why is  $T_{\text{FL}}$  so small in units of the bandwidth? This “naturalness problem” is a central problem of condensed matter physics which has attracted considerable attention in the community. Its solution should also provide a clue as to what reference system should be used to describe the anomalous behavior observed in a broad energy regime above  $T_{\text{FL}}$ , when no other instabilities such as magnetism or superconductivity intervene.

Two different directions have been followed to address this puzzle. The first invokes the proximity to quantum critical points (QCPs) [21–23], signaling the transition to an ordered phase, or to an unconventional one such as fractionalized Mott insulators [24,25]. An alternative starting point has been provided by the development of the combination of *ab initio* electronic structure and dynamical mean field theory (LDA + DMFT) [26–29]. Here, the excitations of a solid are understood in terms of atomic

multiplets embedded in an effective medium, and the evolution of the electronic structure from atomic multiplet excitations into quasiparticles arises naturally as temperature is lowered. This approach has provided quantitative predictions in many materials of interest [3,19,28,30–36], where the *ab initio* LDA + DMFT calculations are in surprisingly good agreement with experiments. However, the solution of the LDA + DMFT equations is a complex problem, which generically yields a nonzero FL scale. Hence no connection with the ideas of QCPs was made. The question of how to reduce the FL scale to exactly zero and how to characterize the ensuing anomalous behavior above  $T_{\text{FL}}$  has remained open.

In this Letter, we provide an answer to this question by computing a global phase diagram of the simplest three-channel spin-orbital Kondo model which captures the essential physics of Hund metals, using the exact numerical renormalization group (NRG) method [37]. By tuning the spin or spin-orbital Kondo couplings into the ferromagnetic regimes, we push  $T_{\text{FL}}$  to be exactly zero and identify QCPs. We find quantum phase transitions to a singular-Fermi-liquid (SFL) phase and to a novel non-Fermi-liquid (NFL) phase showing frustrated behavior of alternating overscreenings in spin and orbital sectors, with universal power laws in dynamical susceptibilities. We use conformal field theory (CFT) arguments [38–43] to identify the nature of the NFL phase, analytically reproduce the NRG eigenlevel spectra and explain the power laws. Our global phase diagram provides a clear picture for understanding the

suppression of coherence in Hund metals in terms of proximity to QCPs.

**Model and methods.**—We study the three-channel spin-orbital Kondo (3soK) model derived from a realistic Anderson impurity model in [20,44] for the studies of Hund metals.  $H_{\text{bath}} = \sum_{p m \sigma} \varepsilon_p \psi_{p m \sigma}^\dagger \psi_{p m \sigma}$  describes a symmetric, flat-band bath with half-bandwidth  $D = 1$ , where  $\psi_{p m \sigma}^\dagger$  creates an electron with momentum  $p$  and spin  $\sigma$  in orbital  $m \in \{1, 2, 3\}$ . The bath couples to the impurity spin  $\mathbf{S}$  and orbital isospin  $\mathbf{T}$  via

$$H_{\text{int}} = J_0 \mathbf{S} \cdot \mathbf{J}_{\text{sp}} + K_0 \mathbf{T} \cdot \mathbf{J}_{\text{orb}} + I_0 \mathbf{S} \cdot \mathbf{J}_{\text{sp-orb}} \cdot \mathbf{T}. \quad (1)$$

Here  $\mathbf{S}$  are SU(2) generators in the  $S = 1$  representation, normalized as  $\text{Tr}(S^\alpha S^\beta) = \frac{1}{2} \delta_{\alpha\beta}$ , and  $\mathbf{T}$  are SU(3) generators in the  $\bar{3}$ , i.e., (01) representation [45] (orbital angular momentum takes  $L = 1$  in this representation), and  $\text{Tr}(T^a T^b) = \frac{1}{2} \delta_{ab}$ .  $\mathbf{J}_{\text{sp}}$ ,  $\mathbf{J}_{\text{orb}}$ , and  $\mathbf{J}_{\text{sp-orb}}$  are the bath spin, orbital and spin-orbital densities at the impurity site, with  $J_{\text{sp}}^\alpha = \psi_{m\sigma}^\dagger \frac{1}{2} \sigma_{\sigma\sigma'}^\alpha \psi_{m\sigma'}$ ,  $J_{\text{orb}}^a = \psi_{m\sigma}^\dagger \frac{1}{2} \tau_{mm'}^a \psi_{m'\sigma}$ ,  $J_{\text{sp-orb}}^{a,\alpha} = \frac{1}{4} \psi_{m\sigma}^\dagger \sigma_{\sigma\sigma'}^\alpha \tau_{mm'}^a \psi_{m'\sigma'}$  (summation over repeated indices is implied) and normalized  $\psi_{m\sigma}^\dagger = (1/\sqrt{N}) \sum_p \psi_{p m \sigma}^\dagger$ , and  $\sigma^\alpha [\tau^a]$  are Pauli [Gell-Mann] matrices, with normalization  $\text{Tr}(\sigma^\alpha \sigma^\beta) = 2 \delta_{\alpha\beta}$  [ $\text{Tr}(\tau^a \tau^b) = 2 \delta_{ab}$ ].  $J_0$ ,  $K_0$  and  $I_0$  are bare spin, orbital and spin-orbital Kondo exchange couplings, and we treat them as independent parameters with positive and negative values describing antiferromagnetic (AFM) and ferromagnetic (FM) couplings, respectively. We take  $K_0 = 0.3$  throughout.

We use the full-density-matrix NRG [46] method to solve this model, exploiting its full  $U(1)_{\text{ch}} \times SU(2)_{\text{sp}} \times SU(3)_{\text{orb}}$  symmetry using QSpace [45]. Symmetry labels  $Q \equiv [q, S, (\lambda_1 \lambda_2)]$  are used to label multiplets, where  $q$  is the bath particle number relative to half-filling of the bath (we choose  $q_{\text{imp}} = 0$  because the impurity site has no charge dynamics),  $S$  is the total spin, and  $(\lambda_1 \lambda_2)$  labels an SU(3) representation described by a Young diagram with  $\lambda_1 + \lambda_2$  ( $\lambda_2$ ) boxes in its first (second) row. The impurity multiplet has  $Q_{\text{imp}} = [0, 1, (01)]$ . The bath is discretized logarithmically and mapped to a semi-infinite ‘‘Wilson chain’’ with exponentially decaying hoppings, and the impurity coupled to chain site  $k = 0$ . The chain is diagonalized iteratively while discarding high-energy states, thereby enlarging the low-energy properties: the finite-size level spacing of a chain ending at site  $k \geq 0$  is of order  $\omega_k \propto \Lambda^{-k/2}$ . Here  $\Lambda > 1$  is a discretization parameter, chosen to be 4 in this work. The RG flow can be visualized by combining the rescaled low-lying NRG eigenlevel spectra,  $E = (\mathcal{E} - \mathcal{E}_{\text{ref}})/\omega_k$  vs  $\omega_k$ , with increasing even or odd  $k$ . The imaginary part of the impurity dynamical susceptibilities  $\chi_{\text{sp}}^{\text{imp}}$ ,  $\chi_{\text{orb}}^{\text{imp}}$  and  $\chi_{\text{sp-orb}}^{\text{imp}}$  were calculated at temperature  $T = 10^{-16}$ . Computational details are presented in the Supplemental Material [47].

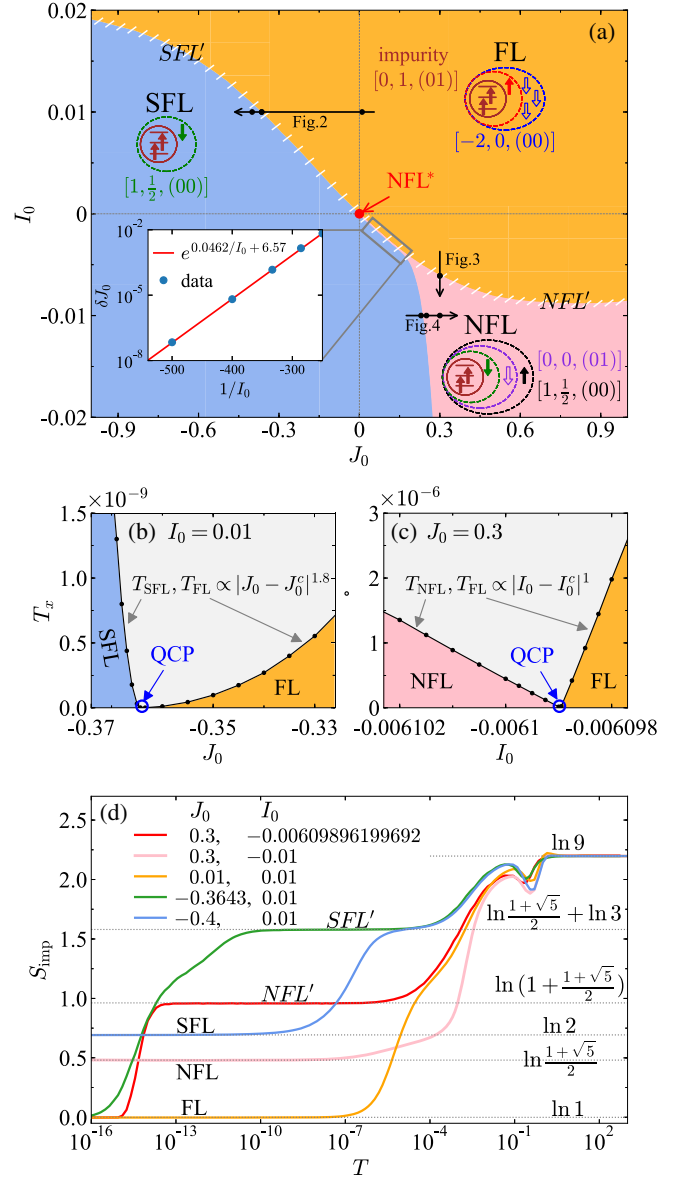


FIG. 1. (a) The calculated global phase diagram vs  $J_0$  and  $I_0$  at fixed  $K_0 = 0.3$ . Four low-energy fixed points are found: Fermi-liquid (FL, orange region); singular Fermi-liquid (SFL, blue region) with underscreened spin and fully screened orbital isospin; frustrated non-Fermi-liquid (NFL, pink region) with alternating spin and orbital overscreenings; and non-Fermi-liquid NFL\* (red dot at  $J_0 = 0, I_0 = 0$ ) with overscreened orbital isospin and degenerate impurity spin  $\frac{1}{2}, \frac{3}{2}$ . Cartoons depict the respective screening processes, where one dashed ellipse loosely represents an even number of Wilson shells. The indicated additional charge then is relative to half-filling, where filled (empty) arrows represent electrons (holes) with corresponding spin direction. The white-hatched region indicates the existence of an intermediate-energy crossover regime SFL' (NFL') enclosing the phase boundary between FL and SFL (NFL). The inset shows the ‘‘funnel width,’’  $\delta J_0$ , of the NFL phase vs  $1/I_0$  when  $I_0 \rightarrow 0^-$ . (b),(c) The onset energy scales  $T_x$  for ( $x =$ ) FL, SFL and NFL vs (b)  $J_0$  or (c)  $I_0$ , where quantum critical points are identified. (d) Impurity contribution to entropy  $S_{\text{imp}}$  as functions of temperature  $T$ .

*Fixed points.*—The calculated global phase diagram as a function of  $J_0$  and  $I_0$  is shown in Fig. 1(a). We first describe the low-energy fixed points found in the phase diagram. Throughout the entire regions where all three Kondo couplings are AFM, and for part of regions where  $J_0$  or  $I_0$  takes FM values (orange region), the system flows to a low-energy FL fixed point. This is seen in the NRG flow diagram and dynamical impurity susceptibilities  $\chi^{\text{imp}}$  at  $J_0 = I_0 = 0.01$  in Figs. 2(a) and 2(d). The ground state is a spin and orbital singlet, with impurity entropy  $S_{\text{imp}} = \ln 1$  [orange curve in Fig. 1(d)]. For small  $\omega$ , all  $\chi^{\text{imp}}$  follow a  $\omega$ -linear behavior, characteristic of a FL.

When  $J_0$  takes FM values and  $I_0$  FM or small AFM values (blue region), the phase is governed by a low-energy SFL [48,58,59] fixed point where the spin is underscreened while the orbitals are fully screened. The transition from FL to SFL is analyzed in Fig. 2 for  $I_0 = 0.01$ . Figures 2(c) and 2(f), computed for  $J_0 = -0.4$ , show the NRG flow and  $\chi^{\text{imp}}$  to the SFL fixed point. It has ground state  $[+1, \frac{1}{2}, (00)]$  and  $S_{\text{imp}}$  approaches  $\ln 2$  at low energies [blue curve in Fig. 1(d)], signaling a residual spin of  $\frac{1}{2}$ .  $\chi_{\text{sp}}^{\text{imp}}$  deviates slightly from a pure  $\omega^{-1}$  power-law by a logarithmic correction at high energy and can be fitted by  $\sim 1/[\omega \ln^2(\omega/T_{\text{SFL}})]$  with  $T_{\text{SFL}}$  as an onset energy scale, consistent with the SFL results in [48].  $\chi_{\text{orb}}^{\text{imp}}$  shows  $\omega$ -linear behavior at low energy, indicating fully screened orbital isospin. The coefficient of the impurity specific heat,  $C_{\text{imp}}(T)/T$  [47], shows divergent behavior [58], confirming the singular nature of this fixed point.

When  $I_0$  takes strong FM and  $J_0$  strong AFM couplings (pink region), we find a novel NFL fixed point, showing very interesting frustrated behavior of alternating overscreenings in spin and orbital sectors. Figure 3 analyzes the transition from FL to NFL at  $J_0 = 0.3$ . Figures 3(c),

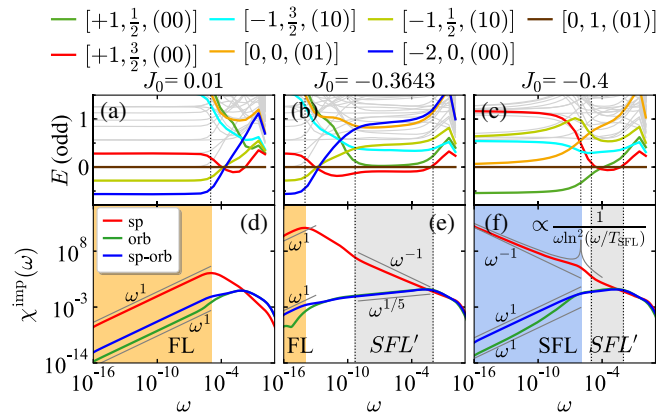


FIG. 2. The phase transition from FL to SFL at  $I_0 = 0.01$ . (a)–(c) NRG flow diagrams of a Wilson chain with odd length  $k$ , with the energy of the lowest  $[0,1,(01)]$  multiplet as the reference energy  $\mathcal{E}_{\text{ref}}$ . The symmetry labels of selected multiplets are shown on top. (d)–(f) Impurity dynamical susceptibility  $\chi^{\text{imp}}(\omega)$ .

3(f), 4(c), and 4(f) show the NRG flow and  $\chi^{\text{imp}}$  towards the NFL fixed point. The two lowest multiplets with either orbital singlet,  $[+1, \frac{1}{2}, (00)]$ , or spin singlet,  $[0,0,(01)]$ , are very close in energy. The dynamical susceptibilities follow perfect and universal power laws for the spin ( $\omega^{-1/5}$ ), orbital ( $\omega^{1/5}$ ) and spin-orbital ( $\omega^1$ ) operators. The impurity entropy  $S_{\text{imp}}$  evaluates to  $\ln[(1 + \sqrt{5})/2]$  [pink curve in Fig. 1(d)]. This value can be obtained from Eq. (6) in [49] for a general  $\text{SU}(N)_K$  Kondo model ( $K$  is the number of channels) with  $N = 3$ ,  $K = 2$ ,  $Q = 2$  indicating  $\text{SU}(3)_2$  orbital overscreening, or with  $N = 2$ ,  $K = 3$ ,  $Q = 1$  indicating  $\text{SU}(2)_3$  spin overscreening. Motivated by this, we follow the recently developed  $\text{SU}(2) \times \text{SU}(3)$  CFT approach [43] to identify the nature of this fixed point. Its NRG eigenlevel spectra  $Q' = [q', S', (\lambda'_1, \lambda'_2)]$  can be reproduced by applying either an  $\text{SU}(2)_3$  fusion procedure in the spin sector or an  $\text{SU}(3)_2$  fusion procedure in the orbital sector, i.e., fusing a spectrum of free fermions  $Q = [q, S, (\lambda_1, \lambda_2)]$ , with an effective impurity multiplet labeling either  $Q_{\text{imp}}^{\text{eff}} = [+1, \frac{1}{2}, (00)]$ , or  $Q_{\text{imp}}^{\text{eff}} = [0, 0, (01)]$ . Double fusion of the spectrum  $Q'$  with the conjugate representation of the impurity multiplet,  $\bar{Q}_{\text{imp}}^{\text{eff}} = [-1, \frac{1}{2}, (00)]$  or  $\bar{Q}_{\text{imp}}^{\text{eff}} = [0, 0, (10)]$ , yields the quantum numbers  $Q'' = [q'', S'', (\lambda''_1, \lambda''_2)]$  to characterize the CFT boundary operators, with scaling dimensions  $\Delta$ , determining the behavior of dynamical susceptibilities.

Tables S1–S2 in the Supplemental Material [47] show the CFT results of the fixed point spectra and compare them with the NRG spectra at  $J_0 = 0.3$ ,  $I_0 = -0.01$ . Both fusion procedures yield the same results, which reproduce the NRG spectra very well. The scaling dimension of the leading boundary operator in the spin, orbital and spin-orbital sectors are found to be  $\Delta_{\text{sp}} = \frac{2}{5}$ ,  $\Delta_{\text{orb}} = \frac{3}{5}$  and  $\Delta_{\text{sp-orb}} = 1$ , respectively. They are also consistent with the CFT results in [49] for either a spin  $\text{SU}(2)_3$  Kondo model ( $\Delta_{\text{sp}} = 2/(2+3)$ ,  $\Delta_{\text{orb}} = 3/(2+3)$ ), or an orbital  $\text{SU}(3)_2$  Kondo model ( $\Delta_{\text{sp}} = 2/(3+2)$ ,

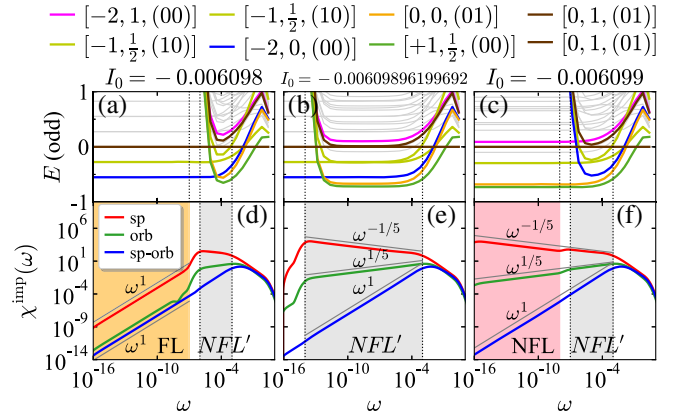


FIG. 3. Analogous to Fig. 2, but for the phase transition from FL to NFL at  $J_0 = 0.3$ .

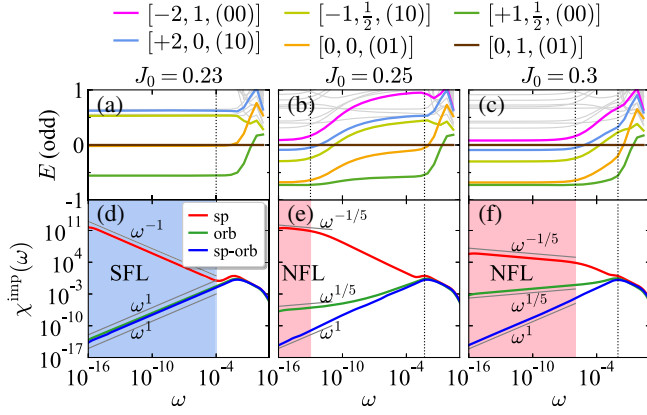


FIG. 4. Analogous to Fig. 2, but for the phase transition from SFL to NFL at  $I_0 = -0.01$ .

$\Delta_{\text{orb}} = 3/(3+2)$ ). The power laws of dynamical susceptibilities can then be understood by the CFT procedure [43]  $\chi_{\text{sp}}^{\text{imp}} \sim \omega^{2\Delta_{\text{sp}}-1} = \omega^{-1/5}$ ,  $\chi_{\text{orb}}^{\text{imp}} \sim \omega^{2\Delta_{\text{orb}}-1} = \omega^{1/5}$  and  $\chi_{\text{sp-orb}}^{\text{imp}} \sim \omega^{2\Delta_{\text{sp-orb}}-1} = \omega^1$ , respectively.

The impurity entropy and the CFT analysis both suggest that the spin  $\text{SU}(2)_3$  and orbital  $\text{SU}(3)_2$  Kondo models with overscreened fixed points are actually equivalent and complementary descriptions of this NFL fixed point. It indicates an alternating spin  $\text{SU}(2)_3$  and orbital  $\text{SU}(3)_2$  overscreening process by successively binding one electron or one hole, as illustrated by the cartoon picture at the bottom right of Fig. 1(a), similar in spirit to that of Nozières and Blandin [60]. To be specific, the strong AFM orbital coupling binds the bare impurity  $Q_{\text{imp}} = [0, 1, (01)]$  and one bath electron  $[+1, \frac{1}{2}, (10)]$  into a fully screened orbital singlet with either spin  $\frac{3}{2}$  or  $\frac{1}{2}$ :  $[0, 1, (01)] \otimes [+1, \frac{1}{2}, (10)] \rightarrow [+1, \frac{3}{2}, (00)] \oplus [+1, \frac{1}{2}, (00)]$ . In the FL phase, the spin  $\frac{3}{2}$  multiplet has the lower energy; it can then bind three holes to form a fully screened spin and orbital singlet [43]:  $[+1, \frac{3}{2}, (00)] \otimes [-3, \frac{3}{2}, (00)] \rightarrow [-2, 0, (00)]$ . By contrast, in the NFL regime, the spin  $\frac{1}{2}$  multiplet has the lower energy since the spin-orbital coupling  $I_0$  is strongly FM. Next, the AFM spin coupling attempts to screen the spin  $\frac{1}{2}$  by coupling it to one hole, to yield a spin singlet,

$$\left[+1, \frac{1}{2}, (00)\right] \otimes \left[-1, \frac{1}{2}, (01)\right] \rightarrow [0, 0, (01)], \quad (2a)$$

but the result is an overscreened orbital isospin. Screening the latter by binding an electron,

$$[0, 0, (01)] \otimes \left[+1, \frac{1}{2}, (10)\right] \rightarrow \left[+1, \frac{1}{2}, (00)\right], \quad (2b)$$

leads back to an overscreened spin. Overall, this results in a never-ending alternation of spin and orbital overscreening, favored by the fact that the multiplets  $[0,0,(01)]$  and

$[+1, \frac{1}{2}, (00)]$  are lowest in energy [see Figs. 3(c), 4(c)], with a very small energy difference.

The special point at  $J_0 = I_0 = 0$  corresponds to an  $\text{SU}(3)_2$  NFL fixed point (NFL\*) with overscreened orbitals and a degenerate impurity spin of  $\frac{1}{2}, \frac{3}{2}$ . The inset of Fig. 1(a) suggests that the region of NFL actually extends to this point. There we analyze the width of the NFL “funnel,” defined by  $\delta J_0 = J_0^{c1} - J_0^{c2}$ , vs  $1/I_0$ , where  $J_0^{c1}$  ( $J_0^{c2}$ ) is the phase boundary between FL (SFL) and NFL. It follows  $\exp(0.0462/I_0 + 6.57)$ , becoming zero only when  $I_0 \rightarrow 0^-$ .

*Phase transitions.*— $T_{\text{FL}}$  on the FL side and  $T_{\text{SFL}}$  ( $T_{\text{NFL}}$ , the NFL scale) on the SFL (NFL) side go to zero as the phase boundary is approached. We find that  $T_{\text{FL}}$ ,  $T_{\text{SFL}}$  and  $T_{\text{NFL}}$  follow power laws as functions of the control parameters  $J_0$  and  $I_0$ ,  $|J_0 - J_0^c|^\alpha$  and  $|I_0 - I_0^c|^\alpha$ , to approach exactly zero at the critical values  $J_0^c$  and  $I_0^c$ , signaling the existence of QCPs [21,22]. The exponents found are  $\alpha = 1.8$  in the FL-SFL transition, and  $\alpha = 1$  for FL-NFL. We show  $T_{\text{FL/SFL}}$  as functions of  $J_0$  at  $I_0 = 0.01$  in Fig. 1(b), and  $T_{\text{FL/NFL}}$  as functions of  $I_0$  at  $J_0 = 0.3$  in Fig. 1(c). More data are shown in Fig. S5 [47].

When approaching the QCP in the FL-SFL transition as in Fig. 2 by decreasing  $J_0$ , the spin-orbital separation window [7,50] increases a lot, as seen in Figs. 2(b) and 2(e) for  $J_0 = -0.3643$ , and a wide crossover regime,  $\text{SFL}'$ , forms at intermediate energies. There the impurity entropy  $S_{\text{imp}}$  evaluates to  $\ln[(1+\sqrt{5})/2] + \ln 3$  [green curve in Fig. 1(d)], corresponding to an orbital overscreened  $\text{SU}(3)_2$  fixed point, coupled to a fluctuating spin-1 moment. This is consistent with the recent findings in the region  $I_0 = 0$  and  $J_0 \rightarrow 0^+$  in [61].  $\chi_{\text{orb}}^{\text{imp}}$  follows a universal power-law of  $\omega^{1/5}$ , showing similarity with the NFL phase due to the same orbital  $\text{SU}(3)_2$  overscreening, while  $\chi_{\text{sp}}^{\text{imp}}$  follows an approximate power law (with some non-power-law corrections, see the Supplemental Material [47]). Across the phase transition, the multiplet  $[+1, \frac{1}{2}, (00)]$  is pushed down to be the new ground state, while the original ground state  $[-2, 0, (00)]$  of the FL phase is pushed up to very high energy.

When approaching the QCP in the FL-NFL transition as illustrated in Fig. 3, the fine-tuning of  $I_0$  generates a large crossover regime  $\text{NFL}'$  at intermediate energies [Figs. 3(b) and 3(e)], where the set of low-lying states is simply the union of those of the FL and NFL spectra (see Table S4 in the Supplemental Material [47]).  $\text{NFL}'$  thus represents a “level-crossing” scenario [47,51,52], involving two orthogonal low-energy subspaces whose levels cross when  $I_0$  is tuned. When sufficiently close, both subspaces contribute to thermodynamic and dynamical properties. Here, the FL and NFL compete in the intermediate-energy regime, and  $I_0$  determines either FL [Figs. 3(a) and 3(d)] or NFL [Figs. 3(c) and 3(f)] to be the low-energy fixed point.

The impurity entropy  $S_{\text{imp}}^{\text{NFL}'}$  evaluates to  $\ln(e^{\chi_{\text{imp}}^{\text{SFL}}} + e^{\chi_{\text{imp}}^{\text{NFL}}}) = \ln\{1 + [(1 + \sqrt{5})/2]\}$  [red curve in Fig. 1(d)], not  $\ln 1 + \ln[(1 + \sqrt{5})/2]$ , because the FL and NFL subspaces do not overlap. Hence the total effective impurity degrees of freedom are the *sum* of the contributions of those two sectors [47].  $\chi_{\text{imp}}^{\text{NFL}'}$  of  $\text{NFL}'$  follow the same power laws as NFL because the NFL part dominates in this regime. For more details on  $\text{NFL}'$ , see the Supplemental Material [47].

The transition from SFL to NFL shown in Fig. 4 confirms the picture of alternating overscreenings. Tuning  $J_0$  to be more AFM, the state  $[0,0,(01)]$  is pushed down to be nearly degenerate with the ground state  $[+1, \frac{1}{2}, (00)]$  [Fig. 4(b)], signaling the start of the alternating overscreening process.  $\chi_{\text{sp}}^{\text{imp}}$  bends downward away from the  $\omega^{-1}$  behavior towards an  $\omega^{-1/5}$  dependence, while  $\chi_{\text{orb}}^{\text{imp}}$  bends upward away from the  $\omega$ -linear behavior towards an  $\omega^{1/5}$  dependence.  $\chi_{\text{sp-orb}}^{\text{imp}}$  still follows  $\omega^1$ .

**Conclusion.**—To summarize, we have presented a global phase diagram of the 3soK model. This allows us to follow the suppression of the coherence scale in Hund metals down to zero energy. The new NFL phase contains the essential ingredients needed to understand the actual incoherent behavior seen above  $T_{\text{FL}}$ . Recent advances in the physics of cold atoms might actually offer a concrete realization of the phase diagram of the model studied. Indeed it has been recently demonstrated that it is possible to simulate  $\text{SU}(N)$  impurity models with tunable exchange interactions reaching both FM and AFM regimes [62,63].

The iron pnictides display an intriguing QCP, as for example in  $\text{BaFe}_2(\text{As}_{1-x}\text{P}_x)_2$  [18,64–66], where a divergent electron mass and concomitant destruction of the FL state was observed. This QCP has motivated several theoretical studies [67–69]. Further progress from the perspective of this work would require the DMFT self-consistency condition and more realistic band structures. In the DMFT treatment of a lattice model, the SFL and the NFL phases are expected to turn into magnetically ordered states, but the impurity model studied here with its power-law singularities would describe the behavior above  $T_{\text{FL}}$ .

The approach presented here, which takes into account the Hund's coupling and the multiorbital nature, is in the same spirit as the ideas of local quantum criticality used to describe Kondo breakdown using impurity models [70], so it would then be also useful for unconventional quantum phase transitions observed in other heavy-fermion materials [71–74]. The global phase diagram of this 3soK model will also have potential impact on the studies of real multi-channel spin and (or) orbital Kondo systems or quantum dots systems, for instance, generalize the studies in [75–79] to three-channel cases.

We thank H. Miao and R. Fernandes for helpful discussion. E. W., K. M. S., and J. vD. are supported by the Deutsche Forschungsgemeinschaft under

Germany's Excellence Strategy–EXC-2111-390814868, and S.-S. B. L. by Grant No. LE3883/2-1. A. W. was supported by the U.S. Department of Energy, Office of Basic Energy Sciences, under Contract No. DE-SC0012704. Y. W. and G. K. were supported by the U.S. Department of Energy, Office of Science, Basic Energy Sciences as a part of the Computational Materials Science Program through the Center for Computational Design of Functional Strongly Correlated Materials and Theoretical Spectroscopy.

- 
- [1] L. D. Landau, E. M. Lifshitz, and L. P. Pitaevskij, in *Statistical Physics: Part 2: Theory of Condensed State*, Landau and Lifshitz Course of Theoretical Physics (Oxford, England, 1980).
  - [2] V. J. Emery and S. A. Kivelson, Superconductivity in Bad Metals, *Phys. Rev. Lett.* **74**, 3253 (1995).
  - [3] Z. P. Yin, K. Haule, and G. Kotliar, Kinetic frustration and the nature of the magnetic and paramagnetic states in iron pnictides and iron chalcogenides, *Nat. Mater.* **10**, 932 (2011).
  - [4] P. Werner, E. Gull, M. Troyer, and A. J. Millis, Spin Freezing Transition and Non-Fermi-Liquid Self-Energy in a Three-Orbital Model, *Phys. Rev. Lett.* **101**, 166405 (2008).
  - [5] L. Medici, J. Mravlje, and A. Georges, Janus-Faced Influence of Hund's Rule Coupling in Strongly Correlated Materials, *Phys. Rev. Lett.* **107**, 256401 (2011).
  - [6] A. Georges, L. Medici, and J. Mravlje, Strong correlations from Hund's coupling, *Annu. Rev. Condens. Matter Phys.* **4**, 137 (2013).
  - [7] K. M. Stadler, G. Kotliar, A. Weichselbaum, and J. von Delft, Hundness versus Mottness in a three-band Hubbard-Hund model: On the origin of strong correlations in Hund metals, *Ann. Phys. (Amsterdam)* **405**, 365 (2019).
  - [8] A. W. Tyler, A. P. Mackenzie, S. Nishizaki, and Y. Maeno, High-temperature resistivity of  $\text{Sr}_2\text{RuO}_4$ : Bad metallic transport in a good metal, *Phys. Rev. B* **58**, R10107 (1998).
  - [9] A. P. Mackenzie, J. W. Reiner, A. W. Tyler, L. M. Galvin, S. R. Julian, M. R. Beasley, T. H. Geballe, and A. Kapitulnik, Observation of quantum oscillations in the electrical resistivity of  $\text{SrRuO}_3$ , *Phys. Rev. B* **58**, R13318 (1998).
  - [10] M. Schneider, D. Geiger, S. Esser, U. S. Pracht, C. Stingl, Y. Tokiwa, V. Moshnyaga, I. Sheikin, J. Mravlje, M. Scheffler, and P. Gegenwart, Low-Energy Electronic Properties of Clean  $\text{CaRuO}_3$ : Elusive Landau Quasiparticles, *Phys. Rev. Lett.* **112**, 206403 (2014).
  - [11] J. Mravlje, M. Aichhorn, T. Miyake, K. Haule, G. Kotliar, and A. Georges, Coherence-Incoherence Crossover and the Mass-Renormalization Puzzles in  $\text{Sr}_2\text{RuO}_4$ , *Phys. Rev. Lett.* **106**, 096401 (2011).
  - [12] T. Kondo, M. Ochi, M. Nakayama, H. Taniguchi, S. Akebi, K. Kuroda, M. Arita, S. Sakai, H. Namatame, M. Taniguchi, Y. Maeno, R. Arita, and S. Shin, Orbital-Dependent Band Narrowing Revealed in an Extremely Correlated Hund's Metal Emerging on the Topmost Layer of  $\text{Sr}_2\text{RuO}_4$ , *Phys. Rev. Lett.* **117**, 247001 (2016).

- [13] X. Deng, K. Haule, and G. Kotliar, Transport Properties of Metallic Ruthenates: A DFT + DMFT Investigation, *Phys. Rev. Lett.* **116**, 256401 (2016).
- [14] Y. Kamihara, T. Watanabe, M. Hirano, and H. Hosono, Iron-based layered superconductor  $\text{La}[\text{O}_{1-x}\text{F}_x]\text{FeAs}$  ( $x = 0.05\text{--}0.12$ ) with  $T_c = 26$  K, *J. Am. Chem. Soc.* **130**, 3296 (2008).
- [15] G. R. Stewart, Superconductivity in iron compounds, *Rev. Mod. Phys.* **83**, 1589 (2011).
- [16] F. Hardy, A. E. Böhrer, D. Aoki, P. Burger, T. Wolf, P. Schweiss, R. Heid, P. Adelmann, Y. X. Yao, G. Kotliar, J. Schmalian, and C. Meingast, Evidence of Strong Correlations and Coherence-Incoherence Crossover in the Iron Pnictide Superconductor  $\text{KFe}_2\text{As}_2$ , *Phys. Rev. Lett.* **111**, 027002 (2013).
- [17] M. Yi, D. H. Lu, R. Yu, S. C. Riggs, J.-H. Chu, B. Lv, Z. K. Liu, M. Lu, Y.-T. Cui, M. Hashimoto, S.-K. Mo, Z. Hussain, C. W. Chu, I. R. Fisher, Q. Si, and Z.-X. Shen, Observation of Temperature-Induced Crossover to an Orbital-Selective Mott Phase in  $\text{A}_x\text{Fe}_{2-y}\text{Se}_2$  ( $\text{A} = \text{K}, \text{Rb}$ ) Superconductors, *Phys. Rev. Lett.* **110**, 067003 (2013).
- [18] P. Walmsley, C. Putzke, L. Malone, I. Guillaumon, D. Vignolles, C. Proust, S. Badoux, A. I. Coldea, M. D. Watson, S. Kasahara, Y. Mizukami, T. Shibauchi, Y. Matsuda, and A. Carrington, Quasiparticle Mass Enhancement Close to the Quantum Critical Point in  $\text{BaFe}_2(\text{As}_{1-x}\text{P}_x)_2$ , *Phys. Rev. Lett.* **110**, 257002 (2013).
- [19] K. Haule and G. Kotliar, Coherence-incoherence crossover in the normal state of iron oxypnictides and importance of Hund's rule coupling, *New J. Phys.* **11**, 025021 (2009).
- [20] Z. P. Yin, K. Haule, and G. Kotliar, Fractional power-law behavior and its origin in iron-chalcogenide and ruthenate superconductors: Insights from first-principles calculations, *Phys. Rev. B* **86**, 195141 (2012).
- [21] S. Sachdev, Quantum criticality: Competing ground states in low dimensions, *Science* **288**, 475 (2000).
- [22] S. Sachdev, Quantum phase transitions, in *Handbook of Magnetism and Advanced Magnetic Materials* (Wiley-Interscience, New Jersey, 2007).
- [23] S. Sachdev, *Quantum Phase Transitions*, 2nd ed. (Cambridge University Press, Cambridge, England, 2011).
- [24] S. Sachdev, Understanding correlated electron systems by a classification of mott insulators, *Ann. Phys. (Amsterdam)* **303**, 226 (2003).
- [25] D.-H. Lee and J. M. Leinaas, Mott Insulators Without Symmetry Breaking, *Phys. Rev. Lett.* **92**, 096401 (2004).
- [26] A. Georges, G. Kotliar, W. Krauth, and M. J. Rozenberg, Dynamical mean-field theory of strongly correlated fermion systems and the limit of infinite dimensions, *Rev. Mod. Phys.* **68**, 13 (1996).
- [27] A. I. Lichtenstein, M. I. Katsnelson, and G. Kotliar, Finite-Temperature Magnetism of Transition Metals: An ab initio Dynamical Mean-Field Theory, *Phys. Rev. Lett.* **87**, 067205 (2001).
- [28] M. Aichhorn, L. Pourovskii, V. Vildosola, M. Ferrero, O. Parcollet, T. Miyake, A. Georges, and S. Biermann, Dynamical mean-field theory within an augmented plane-wave framework: Assessing electronic correlations in the iron pnictide  $\text{LaFeAsO}$ , *Phys. Rev. B* **80**, 085101 (2009).
- [29] K. Haule, C.-H. Yee, and K. Kim, Dynamical mean-field theory within the full-potential methods: Electronic structure of  $\text{CeIrIn}_5$ ,  $\text{CeCoIn}_5$ , and  $\text{CeRhIn}_5$ , *Phys. Rev. B* **81**, 195107 (2010).
- [30] G. Kotliar, S. Y. Savrasov, K. Haule, V. S. Oudovenko, O. Parcollet, and C. A. Marianetti, Electronic structure calculations with dynamical mean-field theory, *Rev. Mod. Phys.* **78**, 865 (2006).
- [31] J. H. Shim, K. Haule, and G. Kotliar, Fluctuating valence in a correlated solid and the anomalous properties of  $\delta$ -plutonium, *Nature (London)* **446**, 513 (2007).
- [32] K. Haule, J. H. Shim, and G. Kotliar, Correlated Electronic Structure of  $\text{LaO}_{1-x}\text{F}_x\text{FeAs}$ , *Phys. Rev. Lett.* **100**, 226402 (2008).
- [33] K. Haule and G. Kotliar, Arrested Kondo effect and hidden order in  $\text{URu}_2\text{Si}_2$ , *Nat. Phys.* **5**, 796 (2009).
- [34] X. Deng, A. Sternbach, K. Haule, D. N. Basov, and G. Kotliar, Shining Light on Transition-Metal Oxides: Unveiling the Hidden Fermi Liquid, *Phys. Rev. Lett.* **113**, 246404 (2014).
- [35] H. Shinaoka, S. Hoshino, M. Troyer, and P. Werner, Phase Diagram of Pyrochlore Iridates: All-In–All-Out Magnetic Ordering and Non-Fermi-Liquid Properties, *Phys. Rev. Lett.* **115**, 156401 (2015).
- [36] M. Kim, J. Mravlje, M. Ferrero, O. Parcollet, and A. Georges, Spin-Orbit Coupling and Electronic Correlations in  $\text{Sr}_2\text{RuO}_4$ , *Phys. Rev. Lett.* **120**, 126401 (2018).
- [37] R. Bulla, T. A. Costi, and T. Pruschke, Numerical renormalization group method for quantum impurity systems, *Rev. Mod. Phys.* **80**, 395 (2008).
- [38] I. Affleck, A current algebra approach to the Kondo effect, *Nucl. Phys.* **B336**, 517 (1990).
- [39] I. Affleck and A. W. W. Ludwig, The Kondo effect, conformal field theory and fusion rules, *Nucl. Phys.* **B352**, 849 (1991).
- [40] I. Affleck and A. W. W. Ludwig, Critical theory of overscreened Kondo fixed points, *Nucl. Phys.* **B360**, 641 (1991).
- [41] I. Affleck and A. W. W. Ludwig, Exact conformal-field-theory results on the multichannel Kondo effect: Single-fermion Green's function, self-energy, and resistivity, *Phys. Rev. B* **48**, 7297 (1993).
- [42] A. W. W. Ludwig and I. Affleck, Exact conformal-field-theory results on the multi-channel Kondo effect: Asymptotic three-dimensional space- and time-dependent multi-point and many-particle Green's functions, *Nucl. Phys.* **B428**, 545 (1994).
- [43] E. Walter, K. M. Stadler, S. S. B. Lee, Y. Wang, G. Kotliar, A. Weichselbaum, and J. von Delft, Uncovering non-fermi-liquid behavior in Hund metals: Conformal field theory analysis of a  $\text{SU}(2) \times \text{SU}(3)$  spin-orbital Kondo model, [arXiv:1908.04362](https://arxiv.org/abs/1908.04362).
- [44] C. Aron and G. Kotliar, Analytic theory of Hund's metals: A renormalization group perspective, *Phys. Rev. B* **91**, 041110(R) (2015).
- [45] A. Weichselbaum, Non-Abelian symmetries in tensor networks: A quantum symmetry space approach, *Ann. Phys. (Amsterdam)* **327**, 2972 (2012).
- [46] A. Weichselbaum and J. von Delft, Sum-Rule Conserving Spectral Functions from the Numerical Renormalization Group, *Phys. Rev. Lett.* **99**, 076402 (2007).

- [47] See the Supplemental Material at <http://link.aps.org/supplemental/10.1103/PhysRevLett.124.136406> for computational details, more NRG flow diagrams and dynamical susceptibilities in Sec. S-I, more data of  $T_{FL}$ ,  $T_{SFL}$ , and  $T_{NFL}$  as functions of  $J_0$  and  $I_0$  in Sec. S-II, CFT analysis in Sec. S-III, the detailed interpretation the “level-crossing” scenario and a proof of the impurity entropy  $S_{imp}$  of  $NFL'$  in Sec. S-IV, the impurity spectral functions  $A_r(\omega)$  in Sec. S-V, the coefficients of specific heat  $\gamma(T)$  in Sec. S-VI, the impurity static susceptibilities for SFL and NFL phases in Sec. S-VII, the energy difference of multiplets  $[+1, \frac{1}{2}, (00)]$  and  $[+1, \frac{3}{2}, (00)]$  along the phase boundary in Sec. S-VIII, the justification of the 3soK model in Sec. S-IX, the dependence on the discretization parameter  $\Lambda$  in Sec. S-X, and the irreducible representations of SU(3) in Sec. S-XI. The Supplemental Material includes Refs. [7,43,48–57].
- [48] W. Koller, A. C. Hewson, and D. Meyer, Singular dynamics of underscreened magnetic impurity models, *Phys. Rev. B* **72**, 045117 (2005).
- [49] O. Parcollet, A. Georges, G. Kotliar, and A. Sengupta, Overscreened multichannel SU( $N$ ) Kondo model: Large- $N$  solution and conformal field theory, *Phys. Rev. B* **58**, 3794 (1998).
- [50] K. M. Stadler, Z. P. Yin, J. von Delft, G. Kotliar, and A. Weichselbaum, Dynamical Mean-Field Theory Plus Numerical Renormalization-Group Study of Spin-Orbital Separation in a Three-Band Hund Metal, *Phys. Rev. Lett.* **115**, 136401 (2015).
- [51] B. Sbierski, M. Hanl, A. Weichselbaum, H. E. Türeci, M. Goldstein, L. I. Glazman, J. von Delft, and A. İmamoğlu, Proposed Rabi-Kondo Correlated State in a Laser-Driven Semiconductor Quantum Dot, *Phys. Rev. Lett.* **111**, 157402 (2013).
- [52] S.-S. B. Lee, J. von Delft, and M. Goldstein, Non-Fermi-liquid Kondo screening under Rabi driving, *Phys. Rev. B* **101**, 085110 (2020).
- [53] T. A. Costi, Kondo Effect in a Magnetic Field and the Magnetoresistivity of Kondo Alloys, *Phys. Rev. Lett.* **85**, 1504 (2000).
- [54] C. Hong, G. Yoo, J. Park, M.-K. Cho, Y. Chung, H.-S. Sim, D. Kim, H. Choi, V. Umansky, and D. Mahalu, Attractive coulomb interactions in a triple quantum dot, *Phys. Rev. B* **97**, 241115(R) (2018).
- [55] A. Hamo, A. Benyamini, I. Shapir, I. Khivrich, J. Waissman, K. Kaasbjerg, Y. Oreg, F. von Oppen, and S. Ilani, Electron attraction mediated by coulomb repulsion, *Nature (London)* **535**, 395 (2016).
- [56] G. Yoo, J. Park, S.-S. B. Lee, and H.-S. Sim, Anisotropic Charge Kondo Effect in a Triple Quantum Dot, *Phys. Rev. Lett.* **113**, 236601 (2014).
- [57] A. Weichselbaum, S. Capponi, P. Lecheminant, A. M. Tsvelik, and A. M. Läuchli, Unified phase diagram of antiferromagnetic SU( $N$ ) spin ladders, *Phys. Rev. B* **98**, 085104 (2018).
- [58] P. Coleman and C. Pépin, Singular fermi liquid behavior in the underscreened Kondo model, *Phys. Rev. B* **68**, 220405 (R) (2003).
- [59] P. Mehta, N. Andrei, P. Coleman, L. Borda, and G. Zarand, Regular and singular fermi-liquid fixed points in quantum impurity models, *Phys. Rev. B* **72**, 014430 (2005).
- [60] Ph. Nozières and A. Blandin, Kondo effect in real metals, *J. Phys. France* **41**, 193 (1980).
- [61] A. Horvat, R. Zitko, and J. Mravlje, Non-fermi-liquid fixed point in multi-orbital Kondo impurity model relevant for Hund’s metals, [arXiv:1907.07100](https://arxiv.org/abs/1907.07100).
- [62] F. Scazza, C. Hofrichter, M. Höfer, P. C. De Groot, I. Bloch, and S. Fölling, Observation of two-orbital spin-exchange interactions with ultracold SU( $N$ )-symmetric fermions, *Nat. Phys.* **10**, 779 (2014).
- [63] L. Riegger, N. D. Opong, M. Höfer, D. R. Fernandes, I. Bloch, and S. Fölling, Localized Magnetic Moments with Tunable Spin Exchange in a Gas of Ultracold Fermions, *Phys. Rev. Lett.* **120**, 143601 (2018).
- [64] S. Jiang, H. Xing, G. Xuan, C. Wang, Z. Ren, C. Feng, J. Dai, Z. Xu, and G. Cao, Superconductivity up to 30 k in the vicinity of the quantum critical point in BaFe<sub>2</sub>(As<sub>1-x</sub>P<sub>x</sub>)<sub>2</sub>, *J. Phys. Condens. Matter* **21**, 382203 (2009).
- [65] S. Kasahara, T. Shibauchi, K. Hashimoto, K. Ikada, S. Tonegawa, R. Okazaki, H. Shishido, H. Ikeda, H. Takeya, K. Hirata, T. Terashima, and Y. Matsuda, Evolution from non-Fermi- to Fermi-liquid transport via isovalent doping in BaFe<sub>2</sub>(As<sub>1-x</sub>P<sub>x</sub>)<sub>2</sub> superconductors, *Phys. Rev. B* **81**, 184519 (2010).
- [66] E. Abrahams and Q. Si, Quantum criticality in the iron pnictides and chalcogenides, *J. Phys. Condens. Matter* **23**, 223201 (2011).
- [67] R. M. Fernandes, S. Maiti, P. Wölfle, and A. V. Chubukov, How Many Quantum Phase Transitions Exist Inside the Superconducting Dome of the Iron Pnictides?, *Phys. Rev. Lett.* **111**, 057001 (2013).
- [68] A. Levchenko, M. G. Vavilov, M. Khodas, and A. V. Chubukov, Enhancement of the London Penetration Depth in Pnictides at the Onset of Spin-Density-Wave Order Under Superconducting Dome, *Phys. Rev. Lett.* **110**, 177003 (2013).
- [69] D. Chowdhury, B. Swingle, E. Berg, and S. Sachdev, Singularity of the London Penetration Depth at Quantum Critical Points in Superconductors, *Phys. Rev. Lett.* **111**, 157004 (2013).
- [70] Q. Si, S. Rabello, K. Ingersent, and J. L. Smith, Locally critical quantum phase transitions in strongly correlated metals, *Nature (London)* **413**, 804 (2001).
- [71] G. R. Stewart, Heavy-fermion systems, *Rev. Mod. Phys.* **56**, 755 (1984).
- [72] H. Takagi, C. Urano, S. Kondo, M. Nohara, Y. Ueda, T. Shiraki, and T. Okubo, Transport properties of metallic LiV<sub>2</sub>O<sub>4</sub> single crystals—heavy mass Fermi liquid behavior, *Mater. Sci. Eng. B* **63**, 147 (1999).
- [73] C. Urano, M. Nohara, S. Kondo, F. Sakai, H. Takagi, T. Shiraki, and T. Okubo, LiV<sub>2</sub>O<sub>4</sub> Spinel as a Heavy-Mass Fermi Liquid: Anomalous Transport and Role of Geometrical Frustration, *Phys. Rev. Lett.* **85**, 1052 (2000).
- [74] P. Gegenwart, Q. Si, and F. Steglich, Quantum criticality in heavy-fermion metals, *Nat. Phys.* **4**, 186 (2008).
- [75] P. Trocha, Orbital kondo effect in double quantum dots, *Phys. Rev. B* **82**, 125323 (2010).
- [76] P. P. Baruselli, R. Requist, M. Fabrizio, and E. Tosatti, Ferromagnetic Kondo Effect in a Triple Quantum Dot System, *Phys. Rev. Lett.* **111**, 047201 (2013).
- [77] L. Zhu, G. Woltersdorf, and J. Zhao, Observation of orbital two-channel Kondo effect in a ferromagnetic L10-MnGa film, *Sci. Rep.* **6**, 34549 (2016).

- [78] L. Pan, Y.D. Wang, Z.H. Li, J.H. Wei, and Y.J. Yan, Kondo effect in double quantum dots with ferromagnetic RKKY interaction, *J. Phys. Condens. Matter* **29**, 025601 (2016).
- [79] Z. Shi, E.M. Nica, and I. Affleck, Kondo effect due to a hydrogen impurity in graphene: A multichannel kondo problem with diverging hybridization, *Phys. Rev. B* **100**, 125158 (2019).